Decoration of WS2 Nanotubes and Fullerene-Like MoS2 with Gold Nanoparticles

ARTICLE *in* THE JOURNAL OF PHYSICAL CHEMISTRY C · JANUARY 2014

Impact Factor: 4.77 · DOI: 10.1021/jp407388h

THE JOURNAL OF PHYSICAL CHEMISTRY C

Article

pubs.acs.org/JPCC

Decoration of WS_2 Nanotubes and Fullerene-Like MoS_2 with Gold Nanoparticles

Alexander Yu. Polyakov,[†] Lena Yadgarov,[‡] Ronit Popovitz-Biro,[§] Vasily A. Lebedev,[†] Iddo Pinkas,[§] Rita Rosentsveig,[‡] Yishay Feldman,[§] Anastasia E. Goldt,[†] Eugene A. Goodilin,*[,†] and Reshef Tenne[‡]

[†]Department of Materials Science, Lomonosov Moscow State University, GSP-1, 1-73 Leninskiye Gory, Laboratory Building B, Moscow, Russia 119991

[‡]Department of Materials and Interfaces and [§]Department of Chemical Research Support, Faculty of Chemistry, Weizmann Institute of Science, Rehovot, Israel 76100

Supporting Information

ABSTRACT: A new technique of gold nanoparticle (AuNP) growth on the sidewalls of WS_2 inorganic nanotubes (INT-WS_2) and the surface of MoS_2 fullerene-like nanoparticles (IF-MoS_2) is developed to produce metal−semiconductor nanocomposites. The coverage density and mean size of the nanoparticles are dependent on the $HAuCl_4$/MS_2 (M = W, Mo) molar ratio. AuNPs formation mechanism seems to involve spatially divided reactions of $AuCl_4^-$ reduction and WS_2/MoS_2 oxidation taking place on the surface defects of the disulfide nanostructures rather than directly at the AuNP-INT/IF interface. A strong epitaxial matching between the lattices of the gold nanoparticles and the INT-WS_2 or IF-MoS_2 seems to suppress plasmon resonance in the nanocomposites with small (<10 nm mean size) AuNPs.

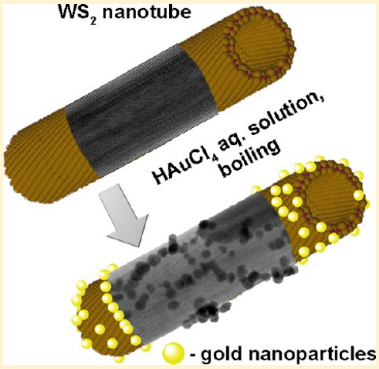

INTRODUCTION

Composite nanostructures based on semiconductors decorated with gold nanoparticles (AuNPs) have attracted growing attention due to their unique optical and electronic properties originated from unusual heterojunctions and the exciton−plasmon coupling.[1] Deposition of AuNPs was used to enhance the photocatalytic activity of TiO_2,[2−4] CeO_2,[5,6] ZnO,[7,8] and ZrO_2[9] nanoparticles. Semiconducting single-walled carbon nanotubes (CNT) decorated with AuNPs were used as H_2S gas sensors.[10] Silicon nanowires−AuNPs hybrid materials are known to be a highly efficient near-infrared hyperthermia agent for cancer cells destruction.[11] Composites based on gold-modified CNT,[12−14] TiO_2 nanotube,[15−17] ZnO nanoneedle, and nanorod arrays[18] were widely studied as prospective SERS-active materials.

Nanocomposites based on carbon and oxide nanotubes require special efforts to establish chemical bonding of the gold nanoparticles to the underlying substrate surface. On the contrary, the surface of nanostructures of layered transition-metal dichalcogenides, like WS_2 and MoS_2, consists of an outer layer of sulfur atoms which are suitable for noble-metal linking due to formation of relatively strong Au−S bonds. This chemical bonding can increase the stability of resulting nanocomposites and facilitate a charge transfer between the AuNPs and the semiconductor.

INT-WS_2 and IF-MoS_2 represent inorganic structures with nested molecular sheets consisting each of six-fold-bonded W or Mo atoms sandwiched between three-fold-bonded sulfur atoms.[19] INT-WS_2 are tubular analogues of multiwalled CNT but composed of WS_2 layers, whereas IF-MoS_2 are closed-caged nanoparticles with a hollow core like in carbon nano-onions. Previous reports concerning the atomic structure of INT-WS_2 and IF-MoS_2 show 2H stacking of the disulfide layers; however, the perfect transitional symmetry of 2H stacking is distorted because the layers are slightly shifted or bent with respect to each other due to shape constraints.[20] Recently, high-resolution transmission electron microscopy (HRTEM) was used to elucidate the structure of disulfide INT/IF.[20,21] It was found that a nearly random sequence of stacking with antiparallel (2H) and parallel (3R) chevrons in adjacent layers is common in these structures. In addition, defects such as boundaries, nonplanar triple layers, dislocations, platelet-like fragments, etc., are usually present in the nanotubes and fullerene-like nanoparticles.[22,23] WS_2 nanotubes and fullerene-like MoS_2 nanoparticles are usually synthesized from WO_3 and MoO_3 nanoparticles, respectively, by reduction with H_2S and N_2/H_2 gases in a fluidized-bed reactor.[24−27] Recently, several studies of INT/IF-WS_2 modification by *n*-octadecyl phosphonic acid (OPA),[28] alkyl-silane derivatives,[29] and semiconductor quantum dots[30] as well as development of core−shell nanostructures based on INT-WS_2 like PbI_2@WS_2,[31] BiI_3@WS_2, SbI_3@WS_2@SbI_3, and WS_2@MoS_2[32] nanotubular structures were reported.

Received: July 25, 2013
Revised: December 18, 2013
Published: January 6, 2014

   dx.doi.org/10.1021/jp407388h | *J. Phys. Chem. C* 2014, 118, 2161−2169

Since the exterior atomic layer of both perfect INT-WS_2 and IF-MoS_2 is presented by sulfur atoms, it can be considered as a "soft" Lewis base and according to Pearson's hard−soft-acid−base (HSAB) principle should have a tendency to be bonded with "soft" Lewis acid cations as well as nanoparticles containing such cations.[33] On the basis of the HSAB principle, functionalization of the INT-WS_2 and IF-MoS_2 nanoparticles surfaces with different moieties becomes possible via multifunctional polymeric ligands containing scorpionate-type nitrilotriacetic acid (NTA) groups partly coordinating Ni^{2+} cations which, in turn, can use their vacant coordination sites for binding to the surface S atoms of the dichalcogenide nanostructures.[34−36] The same principle was used for immobilization of ZnO seeds on the INT-WS_2 and further synthesis of brush-like ZnO-WS_2 nanocomposites[37] as well as for reversible attachment of MnO magnetic nanoparticles to disulfide nanotubes.[38] Metal nanoparticles containing "soft" Lewis acid cations on the surface can also be attached to WS_2 and MoS_2 nanoparticles. It was shown that Pt/Fe_3O_4 Janus nanoparticles easily and irreversible bonded to the INT-WS_2 surface via the "soft" Pt block.[39] Similarly, in-situ-synthesized Ni nanoparticles were attached to INT-MoS_2, resulting in a MoS_2−Ni nanocomposite with a high catalytic activity in hydrodesulfurization of thiophene and its derivatives.[40] Pd nanoseeds were also grown in situ on the surface of INT-WS_2 and served as reactive sites for Co deposition in the synthesis of hybrid Co-coated WS_2 nanotubes. These hybrid nanostructures were shown to exhibit both catalytic reactivity with respect to the hydrodesulfurization reactions[41] and high photocatalytic activity under visible light illumination.[42] The HSAB principle and high thiophilicity of gold were also applied in the previous study focused on modification of INT/IF-WS_2 with presynthesized citrate-capped colloidal gold. Adhesion of AuNPs to WS_2 defects was shown, and the interaction was estimated to be approximately 2 orders of magnitude stronger than the van der Waals forces, implicating strong chemical bonding.[19] However, such coverage was rare and random due to a rather low number of surface defects on the INT-WS_2 and IF-WS_2 surface. In order to produce hybrid nanostructures with an increased coverage density and a controllable nanoparticle size, a new technique for growth of AuNPs directly on the sidewalls of INT-WS_2 and the surface of IF-MoS_2 is developed and discussed in the present work.

EXPERIMENTAL SECTION

INT-WS_2 Decoration with AuNPs. INT-WS_2 were provided by NanoMaterials Ltd. (Israel) and typically of 30−100 nm in diameter and 1−20 μm long. IF-MoS_2 consisting of more than 30 closed MoS_2 shells and having an average size of 70 nm[43] were provided by R. Rosentsveig (Weizmann Institute of Science, Israel). Before modification with AuNPs, nanotubes were deagglomerated in acetone according to a procedure published elsewhere[25] whereas the fullerene-like nanoparticles were used without any pretreatment. The $HAuCl_4 \cdot H_2O$ reagent was purchased from BDH (76862R, GPR, about 50% Au, 1G). All other reactants were of analytical grade. All solutions were prepared using purified water (Milli-Q RG, Millipore). Glassware and magnetic stirring bars utilized for gold nanoparticle synthesis were washed by aqua regia (1:3 HNO_3:HCl mixture). *Caution: aqua regia is an extraordinarily hazardous oxidizing agent and should be handled with extreme care.*

In a typical synthesis of gold nanoparticles on the disulfide nanostructures, 2 mL of freshly prepared aqueous INT-WS_2 suspension (1.3 g/L INT-WS_2) or 1 mL of IF-MoS_2 suspension (1.67 g/L) was added to a hot $HAuCl_4$ aqueous solution of different concentrations and boiled for an additional 3 min under vigorous stirring. For the next 30 min, the reaction mixture was stirred and cooled down to room temperature. The total volume of the reaction mixture was 16 mL, and thus, the overall concentration of disulfides was about 0.65 mM. A series of similar syntheses with different concentrations of $HAuCl_4$ in the reaction mixture was carried out in order to study the influence of the $HAuCl_4/MS_2$ molar ratio (M = W, Mo; ratio range was 1:56−1:1) on the morphology and optical absorption spectra of the AuNP-INT/IF composite nanostructures. A composite with INT-WS_2 was also synthesized using the 2:1 $HAuCl_4/WS_2$ molar ratio. In an additional experiment, INT-WS_2 suspension was added to boiling 0.1 mM $AgNO_3$ solution instead of the $HAuCl_4$ reagent.

In a separate essay, INT-WS_2 suspension in $HAuCl_4$ solution was heated starting from room temperature and then boiled for 3 min in order to clarify the role of adding the nanotube suspension directly into boiling chloroauric acid solution. Room-temperature reactions between $HAuCl_4$ and INT-WS_2 or IF-MoS_2 were also carried out by storage of the disulfide nanostructures in chloroauric acid solution for 3 h at 25 °C. Initially deagglomerated INT-WS_2 without any additional treatment and untreated IF-MoS_2 were used as blanks.

Analytical Methods. Particle morphologies and microstructures were analyzed using TEM and HRTEM techniques. For this purpose, a drop of the reaction product suspension was dripped on polymer/carbon-coated copper grids and then subsequently blotted and dried. Routine TEM measurements were performed using a Philips CM120 microscope operating at 120 kV. HRTEM studies were done using a FEI Tecnai F30 setup operating at 300 kV. STEM-HAADF images, STEM-EELS spectra, and STEM-EDX spectra/maps were obtained using a Carl Zeiss Libra 200 MC microscope operating at 200 kV (0.3 nm spot size in STEM regime) and equipped with an OMEGA energy filter as well as an AZtec EDX system with a X-Max^N 80 mm^2 silicon drift detector. For SEM imaging, a few droplets of the gold-modified INT-WS_2 or IF-MoS_2 suspension were dried at 40 °C onto a clean silicon wafer. Micrographs were taken at 10 kV using Carl Zeiss Leo model Supra (7426) and ULTRA 55 microscopes. Mean particle sizes were estimated using data of typically 300+ particles taken from SEM analysis. XRD data of the suspensions dried on a silicon wafer were collected in a step−scan mode at room temperature using Rigaku TTRAX III and D/MAX 2500 diffractometers equipped with 18 kW rotating anode X-ray sources (Cu Kα radiation, θ−2θ Bragg−Brentano geometry, 10−80° 2θ range, 0.020−0.025° step). XRD spectra were analyzed using STOE WinXPOW and JANA2006 software; for phase identification, the ICDD PDF4 database[44] was used. W and Au content in the liquid phase of the reaction mixtures after growth of AuNPs on INT-WS_2 was studied using inductively coupled plasma mass spectrometry (ICP-MS) by Perkin-Elmer ELAN DRC II apparatus. For complete precipitation of solid components, reaction mixtures were centrifuged (2 times, 30 min, 4000 rpm) before the ICP-MS study and supernatants were separated from the sediments. Signal was collected for ^{182}W, ^{184}W, ^{186}W, and ^{197}Au isotopes.

UV−visible (UV−vis) absorption spectra of the pristine and gold-modified INT-WS_2 and IF-MoS_2 suspensions redispersed

dx.doi.org/10.1021/jp407388h | J. Phys. Chem. C 2014, 118, 2161−2169

by brief (20−30 s) ultrasonic treatment were registered using Perkin-Elmer Lambda 950 spectrophotometer (transmission geometry, wavelength range of 200−900 nm). Three spectra were collected and averaged for each sample in order to ensure reproducibility of the data.

RESULTS AND DISCUSSION

Decoration of INT-WS_2 and IF-MoS_2 with Gold Nanoparticles: The Role of Surface Defects. The technique of the INT-WS_2 or IF-MoS_2 suspension admixed with a boiling $HAuCl_4$ solution produces a dense layer of gold nanoparticles on the sidewalls of INT-WS_2 and the surface of IF-MoS_2 as evident from Figures 1 and 2. As compared to the

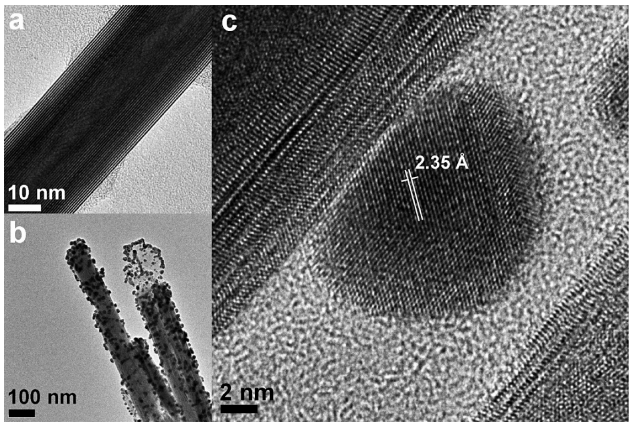

Figure 1. TEM images of a pure WS_2 nanotube (a); WS_2 nanotube decorated with gold nanoparticles (b), and HRTEM of the interface between the WS_2 nanotube and the gold nanoparticle (c); distance between (111) Au planes is shown.

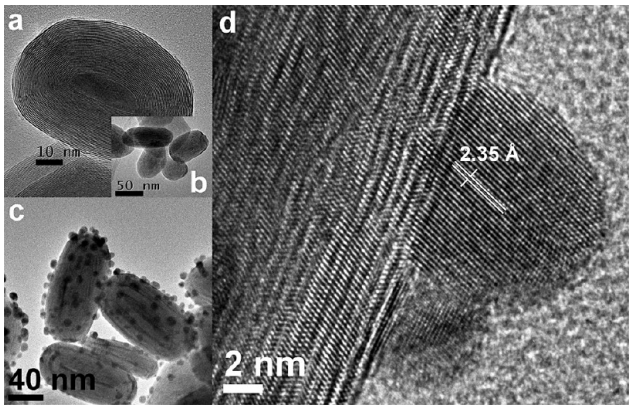

Figure 2. TEM images of a pure IF-MoS_2 in two magnifications (a, b); IF-MoS_2 decorated with gold nanoparticles (c), and HRTEM of the interface between the IF-MoS_2 and the gold nanoparticle (d); distance between (111) Au planes is shown.

original surface of the pristine nanotubes (Figure 1a) and fullerene-like nanoparticles (Figure 2a and 2b), the clearly observed gold nanoparticles were grown and distributed homogeneously on the surface of INT-WS_2 and IF-MoS_2 (Figures 1b and 2c). Nonetheless, the density of AuNPs decorating the nanotube tips and the ledges on the IF surface appears to be higher. The distance between the atomic planes in the grown nanoparticles estimated from high-resolution micrographs (Figures 1c and 2d) is ca. 2.35 Å, which corresponds well to the (111) interplane distance of Au. The presence of metallic gold was also corroborated by the appearance of pronounced (111) Au and (200) Au reflections (ICDD PDF4 entry 00-008-0237, 04-001-2616)[44] in XRD patterns of gold-decorated INT-WS_2 and IF-MoS_2 (Figure 1S, Supporting Information). The local composition of the gold-decorated IF-MoS_2 was also studied with high resolution using STEM-EELS and STEM-EDX point spectra (Figures 2S and 3S, Supporting Information) as well as STEM-EDX mapping (Figure 3), which have clearly shown the presence of gold in the grown nanoparticles and its almost complete absence on the surrounding surface of IF-MoS_2.

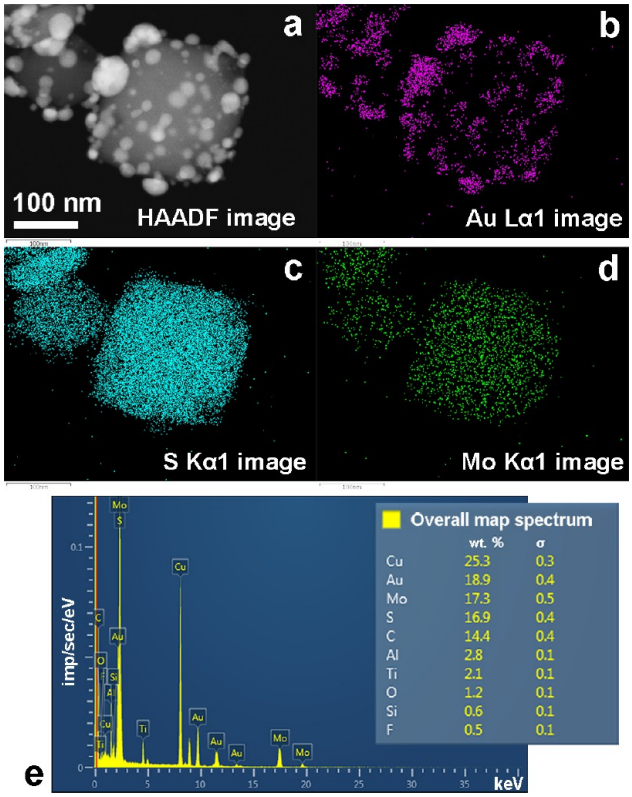

Figure 3. STEM-HAADF image (a), STEM-EDX maps in Au Lα1 (b), S Kα1 (c), and Mo Kα1 (d) signals, and overall map spectrum (e) of the IF-MoS_2 decorated with gold nanoparticles. Presence of high Cu and C signals is due to the copper grid used. Other weak admixing signals are due to the microscope chamber materials.

HRTEM of the interface between the INT-WS_2/IF-MoS_2 and the AuNPs revealed also close interfacial matching of the gold nanoparticles and the disulfide nanostructures. The same is indirectly confirmed by the fact that the shape of the AuNPs deviates from spherical. This observation indicates their direct semispherical growth onto the WS_2 or MoS_2 surface rather than in the volume of the reactant solution. Moreover, closer examination of the interface shows lattice fringe continuation as possibly indicative of epitaxy. Indeed, such a relationship could exist between the (111) planes of Au (0.235 nm) and the (103) planes of WS_2 (0.227 nm) due to a rather small mismatch of 3.5% (Figure 1c). The same is found for the gold nanoparticles on the surface of IF-MoS_2 (Figure 2d). In this case, the observed lattice fringe continuation implies the epitaxial relationship between the (111) planes of Au (0.235 nm) and the (103) planes of MoS_2 (0.228 nm) with an even smaller mismatch of 3.1%. It is worth mentioning that no evidence for

dx.doi.org/10.1021/jp407388h | J. Phys. Chem. C 2014, 118, 2161−2169

oxidation of the disulfide surface in the vicinity of the gold nanoparticles or the presence of interfacial amorphous oxide layers is found by HRTEM. However, it was confirmed that the gold nanoparticles were preferably formed near surface defects of the disulfide nanostructures, e.g., step defects of INT-WS_2 (Figure 4a) and IF-MoS_2 (Figure 4b) as well as defects occurring in the acute edges of the fullerene-like particles (Figure 4c).

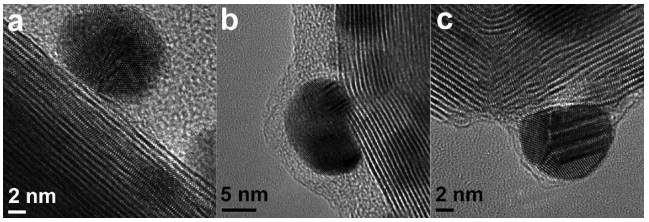

Figure 4. HRTEM micrographs of the gold nanoparticles decorating surface defects of the disulfide nanostructures: AuNPs on step defects of INT-WS_2 (a) and IF-MoS_2 (b); AuNP near discontinuous disulfide layers along the acute edge of IF-MoS_2 (c).

The arrangement of the AuNPs on INT-WS_2/IF-MoS_2 was studied also by SEM. This analysis corroborated preferable growth of the gold nanoparticles near surface defects. It can be clearly seen that AuNPs formed chain-like structures girdling the INT-WS_2 (Figure 5a) or gave characteristic triangle features on the surface of IF-MoS_2 (Figure 5b and 5c). Evidently, the AuNPs outline step or kink defects of INT-WS_2 and triangular IF-MoS_2 facet edges running along the (1−100) face[45] of the crystal.

As observed, such an affinity of the AuNPs with respect to the sulfide-terminated surface defects can be explained by

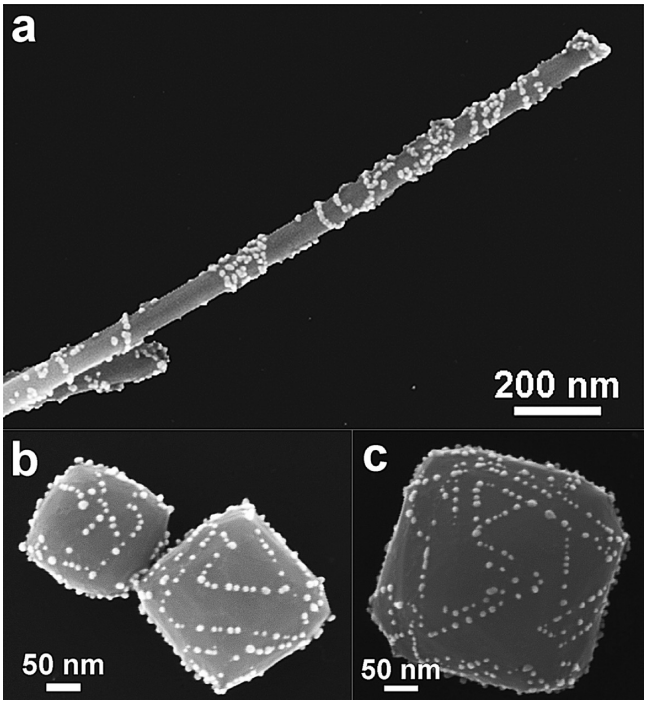

Figure 5. SEM micrographs indicating characteristic arrangement of AuNPs on the surface of the disulfide nanostructures: gold chain-like fragments girdling the INT-WS_2 (a); characteristic triangle features formed from AuNPs decorating the surface of IF-MoS_2 (b, c).

preferable absorption of $AuCl_4^-$ ions from solution onto the defective sites containing unsaturated sulfur atoms. Considering the absence of any oxidized disulfide layers directly on the AuNP-INT/IF interface, it can be suggested that the surface defects of INT-WS_2/IF-MoS_2 serve as an oxidation sites and thus the reduction and oxidation half-reactions are spatially divided due to electron conductivity along the disulfide layers.

In the previous synthesis the nanotubes were added to a boiling chloroauric acid solution. If, instead, the nanotubes were mixed with a room-temperature $HAuCl_4$ solution and then heated and boiled for 3 min, large and irregular-shaped gold particles attached to the tips and major defects (e.g., fractures) of the nanotubes could be observed (Figure 6a). This

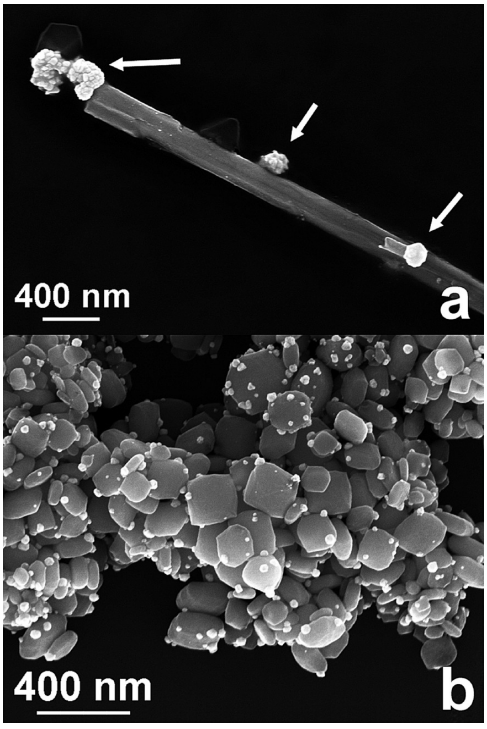

Figure 6. Gold particles grown during heating of INT-WS_2 suspension in $HAuCl_4$ solution starting from room temperature and followed by 3 min boiling (a); arrows denote the irregular-shaped large gold particles formed near the major defects of the nanotube. Gold particles grown on IF-MoS_2 at room temperature (b).

observation suggests that, in this case, a surface reaction between the INT-WS_2 and $HAuCl_4$ takes place during prolonged heating of the reaction mixture until the boiling temperature is reached. The possibility of the room-temperature reaction between $HAuCl_4$ and INT-WS_2 or IF-MoS_2 was also examined by keeping the disulfides dispersed in chloroauric acid solution for 3 h without heating. It was found that, again, a large number of irregular-shaped gold particles formed under these circumstances on the major surface defects of the disulfide nanostructures, e.g., acute edges and vertices of IF-MoS_2 (Figure 6b) usually containing discontinuous MoS_2 layers. Thus, major defects of the disulfide nanostructures are reactive toward gold deposition even at room temperature. However, as indicated from the previous analysis, boiling is necessary for activation of a large number of the reaction sites and thus addition of the INT-WS_2 and IF-MoS_2 directly into boiling $HAuCl_4$ solution is crucial for formation of the large number of gold nuclei on the disulfide nanostructures. Boiling

dx.doi.org/10.1021/jp407388h | J. Phys. Chem. C 2014, 118, 2161−2169

of INT-WS_2 and IF-MoS_2 into $HAuCl_4$–ethanol solution was also attempted but to no avail, indicating the important role of water as a solvent for the reaction mixture.

Effect of $HAuCl_4/MS_2$ Molar Ratio (M = W, Mo) on the Morphology of the Nanocomposites. The effect of the $HAuCl_4/MS_2$ (M = W, Mo) molar ratios in the reaction mixture on the morphology of the gold nanoparticles was studied. Here, a series of experiments with a constant amount of INT-WS_2 and IF-MoS_2 but different concentrations of $HAuCl_4$ was carried out (the range of $HAuCl_4/MS_2$ molar ratios was 1:56–1:1). A clear dependence between the $HAuCl_4/MS_2$ ratio and the mean size of the gold nanoparticles formed on the surface of disulfide nanostructures was observed (Table 1; Figure 4S, Supporting Information). At low $HAuCl_4/MS_2$ ratios (from 1:56 to 1:14), individual AuNPs with a mean size of 4–5 and 6–8 nm were formed and appeared to be randomly distributed on the surface of the INT-WS_2 (Figure 7a) and IF-MoS_2 (Figure 7d), respectively. An increase of the $HAuCl_4/MS_2$ ratio up to 1:8.7–1:4.6 leads to growth of individual AuNPs up to 8–11 nm on INT-WS_2 (Figure 7b) and 10–13 nm on IF-MoS_2 (Figure 7e). In addition, part of the adjacent gold nanoparticles was found to be merged, forming nanoislands and chain-like fragments. At these $HAuCl_4/MS_2$ ratios the aforementioned characteristic arrangement of AuNPs outlining surface defects of the disulfide nanostructures became most apparent. A further increase of the $HAuCl_4/MS_2$ ratio led to growth of gold nanoparticles with a mean size of 30–50 nm and local merging of the AuNPs into large nanoislands and chains on the surface of INT-WS_2 and IF-MoS_2 (Figure 7c and 7f). Many of the individual AuNPs became indiscernible in the formed aggregates. This merging led to an increased width of the size distribution of the gold nanoparticles estimated from statistical analysis of the SEM micrographs. Nonetheless, these large aggregates have a minor influence on the overall size distributions. Moreover, under high $HAuCl_4/MS_2$ ratios, the number of free gold nanoparticles in the suspension increased, indicating dislodging of the AuNPs from the surface of disulfide nanostructures.

Table 1. Mean Size of Individual Gold Nanoparticles Grown on the Surface of INT-WS_2 and IF-MoS_2 by Boiling the Disulfide Nanostructures in Aqueous $HAuCl_4$ Solutions at Different $HAuCl_4/MS_2$ Ratios (M = W, Mo)

	d_{Au}, nm[a]	
$HAuCl_4/MS_2$ molar ratio (M = W, Mo)	gold-modified INT-WS_2	gold-modified IF-MoS_2
1:56	4.0 ± 2.0	6.0 ± 2.0
1:14	5.0 ± 2.5	8.0 ± 2.5
1:8.7	8.0 ± 3.0	10.5 ± 5.5
1:7	8.5 ± 3.0	12.0 ± 5.0
1:4.6	11.0 ± 3.0	13.0 ± 7.5
1:2.3	15.0 ± 5.0	19.0 ± 8.0
1:1	30.0 ± 8.0	35.0 ± 10.0

[a]Size distributions of the individual gold nanoparticles, which can be also merged into gold nanoislands, particularly at high $HAuCl_4/MS_2$ ratios. The dispersion of the reported values is given as the fwhm of a Gaussian distribution fitted to the histograms obtained from analyses of the SEM images.

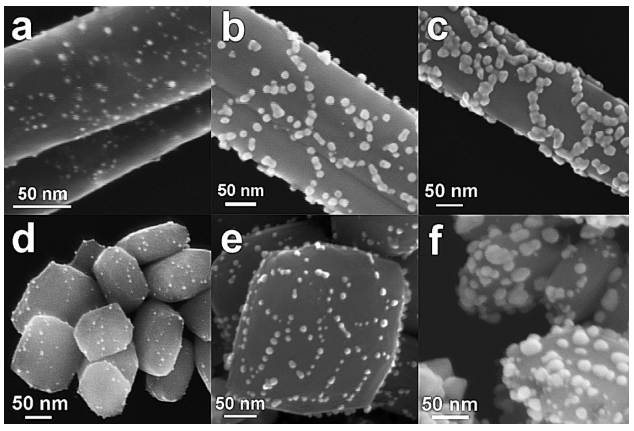

Figure 7. SEM micrographs of the gold-modified INT-WS_2 (a–c) and IF-MoS_2 (d–f) synthesized at 1:56, 1:7, and 1:2.3 $HAuCl_4/MS_2$ (M = W, Mo) molar ratios, respectively.

Thus, variation of the $HAuCl_4/MS_2$ ratio in the reaction mixture allows controlling the mean size of the gold nanoparticles grown on the surface of INT-WS_2 and IF-MoS_2 at least in the 5–35 nm range. Decoration of INT-WS_2 carried out at a $HAuCl_4/WS_2$ molar ratio of 2:1 leads to formation of a dense and virtually continuous layer of gold on the sidewalls of the nanotubes (Figure 5S, Supporting Information). Evidently, a further increase of the $HAuCl_4$ concentration could lead to formation of a continuous gold film on the nanotube surface, i.e., tubular Au-WS_2 core–shell nanocomposites.

Possible Mechanism for Gold Nanoparticles Growth. In order to study the mechanism and byproducts of the reaction between $HAuCl_4$ and WS_2/MoS_2 nanoparticles, chemical analysis of the reaction mixture supernatants was carried out for a series of Au-INT-WS_2 syntheses with a fixed INT-WS_2 amount and different $HAuCl_4$ concentrations. After syntheses, the solid phase of the reaction mixtures was precipitated by centrifugation (2 times, 30 min, 4000 rpm) and the supernatants were analyzed by means of ICP-MS. It was shown that up to 95–99% of the initial gold added to the reaction mixture in the form of $HAuCl_4$ was deposited onto the INT-WS_2. Moreover, 0.45–13% of tungsten from the initial INT-WS_2 appeared to be dissolved during the reaction, and a pronounced dependence was found between the amounts of dissolved W and deposited Au (Figure 6S, Table 1S, Supporting Information) with the slope of a linear fitting equal to 0.136. It is suggested that each WS_2 formula unit formally gives more than 18 electrons for the redox reaction and thus should be oxidized to W^{VI} and S^{VI} compounds, e.g., hydrated WO_3 and SO_4^{2-}. The presence of hydrated WO_3 and H_2WO_4 was confirmed by XRD analysis of a dried reaction mixture after Au-INT-WS_2 nanocomposite synthesis with a $HAuCl_4/WS_2$ molar ratio of 1:1 (Figure 7S, Supporting Information). Thus, a simplified chemical equation for the reaction can be written as

$$6HAuCl_4 + WS_2 + 12H_2O = 6Au + WO_3{\cdot}H_2O + 2H_2SO_4 + 24HCl$$

It is believed that a similar reaction occurs between $AuCl_4^-$ ions with the MoS_2 nanoparticles.

As suggested above, the reduction and oxidation half-reactions in these redox processes are spatially divided due to high electron conductivity of the S–M–S sandwich layers (M = W, Mo). In other words, reduction of $AuCl_4^-$ and gold nucleation can occur at random sites of the disulfide surface due to spontaneous electron transfer from the WS_2 or MoS_2 to

dx.doi.org/10.1021/jp407388h | J. Phys. Chem. C 2014, 118, 2161–2169

the $AuCl_4^-$ ions. The electron deficiency becomes compensated by oxidation of disulfide at the nearest defects and the electron conductivity of the S−M−S sandwich layers. Therefore, the sites near the surface defects became preferable for gold nucleation. The formed gold nuclei seem to be bound with the surface of the disulfides by Au−S bonds conditioning strong fixation of the AuNPs to the INT or IF.

The major defects of the disulfide nanostructures maintain their reactivity even at room temperature. However, addition of INT-WS_2 or IF-MoS_2 directly into the boiling $HAuCl_4$ solution was found to be necessary for formation of a larger amount of reactive sites and thus nucleation of gold nanoparticles on the entire surface of the disulfide nanostructures. Boiling the nanotubes and fullerene-like nanoparticles in acidic solution may also lead to a thorough cleanup of their surfaces and removal of adhered organic passivation layers that are frequently observed on the bare surface.

The driving force for the mentioned electron transfer stems from the difference between the Fermi level of WS_2 and MoS_2 and a rather high reduction potential of $AuCl_4^-$ ($AuCl_4^- + 3e^- = Au + 4Cl^-$). According to previous works,[46−48] the Fermi level of the disulfides is 4.6−4.9 eV below the vacuum level. At the same time, the reduction potential of $AuCl_4^-$ is equal to +1.002 V with respect to the standard hydrogen electrode (SHE) potential, whose absolute potential is known to be from −4.43 to −4.73 V.[49] Thus, the Fermi level of WS_2 and MoS_2 is ca. 0.8 eV higher than the reduction potential of $AuCl_4^-$ (see the scheme in Figure 8), and $AuCl_4^-/WS_2$ and $AuCl_4^-/MoS_2$

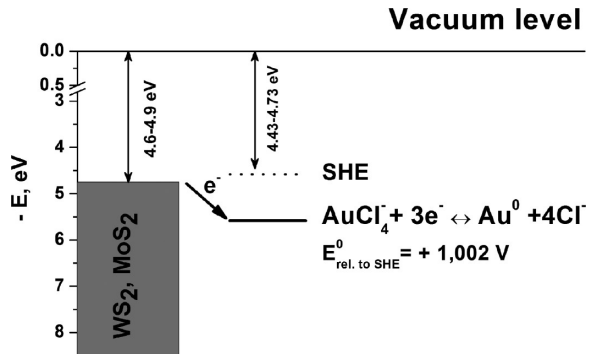

Figure 8. Energy scheme representing the relative positions of WS_2/MoS_2 Fermi levels and reduction potential of the $AuCl_4^-$.

redox couples are formed allowing the spontaneous electron transfer described above. The same mechanism was suggested for spontaneous reduction of $AuCl_4^-$ ions on the surface of carbon nanotubes,[50] graphene,[51,52] and, recently, exfoliated MoS_2 and WS_2 sheets.[53] The suggested mechanism may not be exclusive to gold and could be suitable well for deposition of other noble metals with a low reduction potential of their soluble ions. Indeed, our preliminary experiments have shown that a similar synthesis with $AgNO_3$ solution rather than $HAuCl_4$ leads to formation of Ag nanoparticles on the surface of INT-WS_2 (Figure 8S, Supporting Information). Partial reduction of Pd^{II} ions to Pd^0 on aqueous single-layer MoS_2 dispersions at room temperature was also observed elsewhere.[54]

Optical Properties of Au-INT-WS_2 and Au-IF-MoS_2 Nanocomposites. The optical properties of the pristine and gold-decorated disulfide nanostructures were characterized by UV−vis spectroscopy of their suspensions. Absorption bands in pristine IF-MoS_2 spectrum (Figure 9b, curve 7) at ca. 650 and

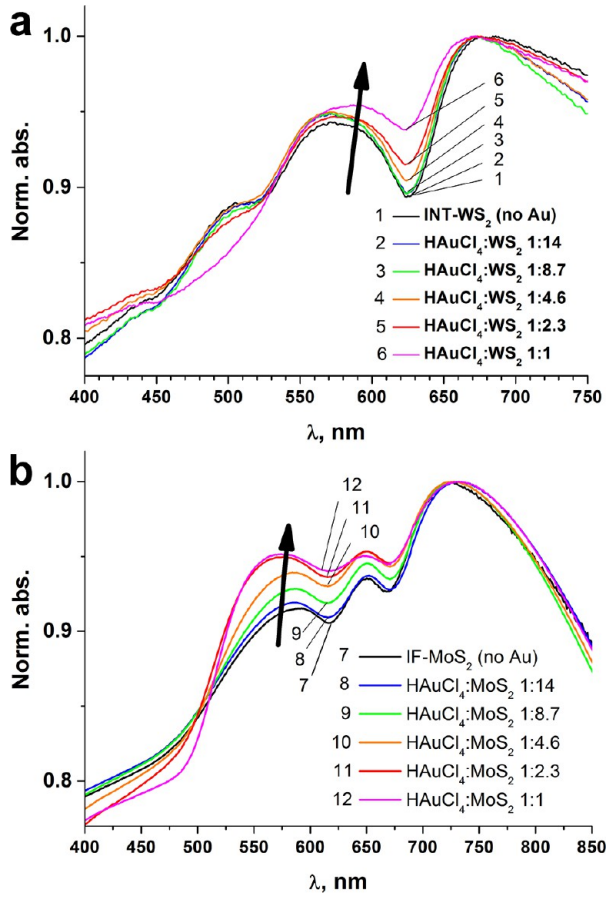

Figure 9. Normalized UV−vis absorption spectra of the gold-modified INT-WS_2 (a) and IF-MoS_2 (b) synthesized at different $HAuCl_4/MS_2$ molar ratios (M = W, Mo). Arrows denote the suggested growth of the surface plasmon resonance peak of the gold nanoparticles with increasing $HAuCl_4/MS_2$ ratio.

580 nm correspond to A1 and B1 excitons, respectively, caused by the $K_4 \rightarrow K_5$ and $K_1 \rightarrow K_5$ transitions at the direct band gap in the K point of the Brillouin zone[55] and slightly (red) shifted in comparison with their positions in bulk MoS_2 due to curvature of S−Mo−S layers and stain. According to a recent study,[56] an intensive peak at ca. 730 nm corresponds to a Mie scattering originating from surface plasmon resonance on IF-MoS_2 nanoparticles in aqueous suspensions. The spectrum of pristine INT-WS_2 film was previously interpreted as consisting of a set of A and B excitonic absorptions at ca. 680 and 570 nm, respectively.[42] However, in analogy to the case of IF-MoS_2 suspensions, there also can be a scattering contribution to the peaks observed in spectrum of INT-WS_2 suspension (Figure 9a, curve 1), and this ambiguity should be a subject of a further research.

The normalized absorption spectra of the samples synthesized with 1:14 and 1:8.7 $HAuCl_4$/INT-WS_2 molar ratios (Figure 9a, curves 2 and 3) were quite similar to the one of the pristine nanotubes. However, at higher $HAuCl_4$/INT-WS_2 ratios (from 1:4.6 to 1:1), increased absorption in the 570−650 nm range leading to blunting of the absorption minimum between the peaks at ca. 680 and 570 nm is observed. These changes can be ascribed to the growing importance of the surface plasmon resonance (SPR) peak of the AuNPs with their increased loading on the INT surface. Analogous variations in the gold-modified IF-MoS_2 spectra are observed (Figure 9b).

dx.doi.org/10.1021/jp407388h | J. Phys. Chem. C 2014, 118, 2161−2169

An increase of the $HAuCl_4/MoS_2$ ratio leads to the growing absorption at 530−670 nm, which can be ascribed to the overlap between the growing SPR peak centered at 550−600 nm (almost coincident with the B exciton peak of MoS_2) with the common IF-MoS_2 spectrum discussed elsewhere.[56] It is well known that the SPR peak of spherical gold nanoparticles with a diameter of 10−50 nm in diluted aqueous sols is centered at 517−533 nm, whereas the increase of the diameter up to 100 nm leads to a red shift of the SPR peak up to 575 nm.[57] However, growth of the nanoparticles directly on the disulfide nanostructures surface leads to a distortion of the spherical shape of AuNPs (Figures 1 and 2) which can cause a red shift of the maximum of the SPR peak from the position typical for free spherical gold nanoparticles. Furthermore, the position and broadening of the SPR peak of AuNPs strongly depend on the effective dielectric constant of the substrate, merging of the nanoparticles, and the interparticle distances.[58−61] In our case, the SPR peak becomes more predominant and slightly shifted to the red region due to growth and merging of the AuNPs for an increased $HAuCl_4/MS_2$ ratio (M = W, Mo).

The noticeable difference between the initial and the gold-modified IF-MoS_2 spectra appears at a lower $HAuCl_4/MS_2$ molar ratio than in the case of INT-WS_2. Considering the mean sizes of the grown AuNPs, as estimated from SEM (Table 1), it can be concluded that the plasmonic features become apparent in the spectra of the nanocomposites when the gold nanoparticles are grown beyond 10 nm in diameter. The absence of Au plasmon peak in samples with <10 nm AuNPs mean size resembles suppression of SPR observed elsewhere[62] in absorption spectra of epitaxially coupled Au/CdS nanocomposites containing small AuNPs. Such a suppression was explained by a "low-barrier" coupling between Au and CdS components, for which Au electrons with energies located above the Fermi level (plasmon band) are not sufficiently confined by the Au/CdS interface to exhibit resonant oscillations. Furthermore, delocalization of the plasma electrons into the CdS counterpart of the nanocomposites occurred leading to suppression of the SPR in AuNPs.[62] Since our HRTEM study (Figures 1 and 2) reveals intimate interfacial matching and epitaxial relationship between the AuNPs and the disulfide nanostructures, the same SPR suppression in Au-INT-WS_2 and Au-IF-MoS_2 nanocomposites can be expected. However, in the discussed work[62] the size of CdS nanorods and Au nanoparticles was controlled precisely whereas both AuNPs and especially the disulfide nanostructures in the present work show a wide size distribution and different types of spatial organization. Therefore, one can conclude that a similar study using INT-WS_2 and IF-MoS_2 with a more narrow size distribution is highly warranted, once such nanoparticles are available.

Thus, UV−vis absorption measurements suggest a possible interesting optoelectronic property of the synthesized composites, namely, suppression of the SPR of gold nanoparticles grown onto the INT-WS_2 or IF-MoS_2 which can be due to "low-barrier" epitaxial coupling of the AuNPs and disulfide nanostructures leading to delocalization of plasma electrons into INT-WS_2 and IF-MoS_2. In addition, since the disulfide nanostructures were found to exhibit their own SPR bands,[56] nanocomposite spectra can also suggest the appearance of collective plasmon oscillations of the AuNPs and the underlying INT/IF.

CONCLUSIONS

Addition of INT-WS_2 or IF-MoS_2 suspension into boiling aqueous solutions of $HAuCl_4$ for a short period of time (3 min) was found to result in heterogeneous growth and effective fixation of either gold nanoparticles or gold nanostructures (e.g., nanoislands and nanochains) onto the surface of the disulfides without any additional reducer, linker, or stabilizer. The experimental conditions allow varying in a desirable manner the number of surface reaction sites and then the mean AuNP size, at least in the range of 5−35 nm. The mechanism of the surface heterogeneous reaction between $HAuCl_4$ and the disulfides seems to involve spatially divided half-reactions of $AuCl_4^-$ reduction and WS_2/MoS_2 oxidation. The interfacial coupling between the gold nanoparticles and INT-WS_2 or IF-MoS_2 seems to lead to suppression of the surface plasmon resonance in the AuNPs with nanoparticles of small sizes grown on the disulfide nanostructures.

ASSOCIATED CONTENT

Supporting Information

XRD patterns of gold-decorated INT-WS_2 and IF-MoS_2; STEM-EELS and STEM-EDX point spectra for gold-decorated IF-MoS_2; graphical representation of the dependence between the $HAuCl_4/MS_2$ molar ratio (M = W, Mo) and the mean size of individual AuNPs decorating the INT-WS_2 and IF-MoS_2; SEM images of the Au-INT-WS_2 nanocomposite synthesized at 2:1 $HAuCl_4$/INT-WS_2 molar ratio; results of ICP-MS analysis of the reaction mixture supernatants; XRD pattern of the reaction mixture dried after the gold-decorated INT-WS_2 synthesis at 1:1 $HAuCl_4/WS_2$ molar ratio; TEM images of silver-decorated INT-WS_2. This material is available free of charge via the Internet at http://pubs.acs.org.

AUTHOR INFORMATION

Corresponding Author

*Phone: +7 495 9394609. Fax: +7 495 9390998. E-mail: goodilin@inorg.chem.msu.ru.

Author Contributions

The manuscript is written through equal contributions of all authors. All authors have given approval to the final version of the manuscript.

Notes

The authors declare no competing financial interest.

ACKNOWLEDGMENTS

The authors are grateful to Dr. Alexey V. Garshev (MSU) for his help in STEM-EELS and STEM-EDX analysis, Dr. Dmitry I. Petukhov (MSU) for his help in ICP-MS measurements, as well as Prof. Dan Oron (Weizmann Institute) for a fruitful discussion. This work was supported by the Israel Science Foundation, Russian Federation for Basic Research (grant 13-03-12190-ofi), and M.V.Lomonosov Moscow State University Program of Development.

ABBREVIATIONS

2H, hexagonal MoS_2/WS_2 polytype; 3R, rhombohedral MoS_2/WS_2 polytype; AuNP, gold nanoparticle; BDH, British Drug Houses Ltd. (merged with Merck KGaA); CNT, carbon nanotubes; EDX, energy-dispersive X-ray spectroscopy; EELS, electron energy loss spectroscopy; ICDD, the International Centre for Diffraction Data; IF, inorganic fullerene/inorganic fullerene-like nanoparticle(s); GPR, general purpose reagent

(equal to Chemically Pure grade); ICP-MS, inductively coupled plasma mass spectrometry; INT, inorganic nanotube(s); HAADF, high-angle annular dark-field [imaging]; HRTEM, high-resolution transmission spectroscopy; HSAB, Hard−Soft-Acid−Base [principle]; NTA, nitrilotriacetic acid/nitrilotriacetate; OPA, *n*-octadecyl phosphonic acid; SERS, surface-enhanced Raman scattering; SHE, standard hydrogen electrode; SPR, surface plasmon resonance; STEM, scanning transmission electron microscopy; TEM, transmission electron microscopy; UV−vis, ultraviolet−visible; XRD, X-ray diffraction

REFERENCES

(1) Ye, J.; Tong, H. Nanoarchitechtonics of Photocatalytic Materials. In *Manipulation of Nanoscale Materials. An Introduction to Nanoarchitectonics*; Ariga, K., Eds.; RSC Publishing: Cambridge, 2012; pp 165−187.

(2) Dawson, A.; Kamat, P. V. Semiconductor-Metal Nanocomposites. Photoinduced Fusion and Photocatalysis of Gold-Capped TiO_2 (TiO_2/Gold) Nanoparticles. *J. Phys. Chem. B* **2001**, *105*, 960−966.

(3) Lee, M.; Amaratunga, P.; Kim, J.; Lee, D. TiO_2 Nanoparticle Photocatalysts Modified with Monolayer-Protected Gold Clusters. *J. Phys. Chem. C* **2010**, *114*, 18366−18371.

(4) Liu, Y.; Chen, L.; Hu, J.; Li, J.; Richards, R. TiO_2 Nanoflakes Modified with Gold Nanoparticles as Photocatalysts with High Activity and Durability Under Near UV Irradiation. *J. Phys. Chem. C* **2010**, *114*, 1641−1645.

(5) Primo, A.; Marino, T.; Corma, A.; Molinari, R.; Garcia, H. Efficient Visible-Light Photocatalytic Water Splitting by Minute Amounts of Gold Supported on Nanoparticulate CeO_2 Obtained by a Biopolymer Templating Method. *J. Am. Chem. Soc.* **2011**, *133*, 6930−6933.

(6) Kominami, H.; Tanaka, A.; Hashimoto, K. Mineralization of Organic Acids in Aqueous Suspensions of Gold Nanoparticles Supported on Cerium(IV) Oxide Powder Under Visible Light Irradiation. *Chem. Commun.* **2010**, *46*, 1287−1289.

(7) Lee, J.; Shim, H. S.; Lee, M.; Song, J. K.; Lee, D. Size-Controlled Electron Transfer and Photocatalytic Activity of ZnO-Au Nanoparticle Composites. *J. Phys. Chem. Lett.* **2011**, *2*, 2840−2845.

(8) Kim, J.; Yong, K. A Facile, Coverage Controlled Deposition of Au Nanoparticles on ZnO Nanorods by Sonochemical Reaction for Enhancement of Photocatalytic Activity. *J. Nanopart. Res.* **2012**, *14*, 1033.

(9) Zhu, H.; Ke, X.; Yang, X.; Sarina, S.; Liu, H. Reduction of Nitroaromatic Compounds on Supported Gold Nanoparticles by Visible and Ultraviolet Light. *Angew. Chem., Int. Ed.* **2010**, *122*, 9851−9855.

(10) Mubeen, S.; Lim, J.-H.; Srirangarajan, A.; Mulchandani, A.; Deshusses, M. A.; Myung, N. V. Gas Sensing Mechanism of Gold Nanoparticles Decorated Single-Walled Carbon Nanotubes. *Electroanalysis* **2011**, *23*, 2687−2692.

(11) Su, Y.; Wei, X.; Peng, F.; Zhong, Y.; Lu, Y.; Su, S.; Xu, T.; Lee, S.-T.; He, Y. Gold Nanoparticles-Decorated Silicon Nanowires as Highly Efficient Near-Infrared Hyperthermia Agents for Cancer Cells Destruction. *Nano Lett.* **2012**, *12*, 1845−1850.

(12) Wang, X.; Wang, C.; Cheng, L.; Lee, S.-T.; Liu, Z. Noble Metal Coated Single-Walled Carbon Nanotubes for Applications in Surface Enhanced Raman Scattering Imaging and Photothermal Therapy. *J. Am. Chem. Soc.* **2012**, *134*, 7414−7422.

(13) Demeritte, T.; Kanchanapally, R.; Fan, Z.; Singh, A. K.; Senapati, D.; Dubey, M.; Zakarb, E.; Ray, P. C. Highly Efficient SERS Substrate for Direct Detection of Explosive TNT Using Popcorn-Shaped Gold Nanoparticle-Functionalized SWCNT Hybrid. *Analyst* **2012**, *137*, 5041−5045.

(14) Beqa, L.; Singh, A. K.; Fan, Z.; Senapati, D.; Ray, P. C. Chemically Attached Gold Nanoparticle−Carbon Nanotube Hybrids for Highly Sensitive SERS Substrate. *Chem. Phys. Lett.* **2011**, *512*, 237−242.

(15) Roguska, A.; Kudelski, A.; Pisarek, M.; Opara, M.; Janik-Czachor, M. Surface-Enhanced Raman Scattering (SERS) Activity of Ag, Au and Cu Nanoclusters on TiO_2-Nanotubes/Ti Substrate. *Appl. Surf. Sci.* **2011**, *257*, 8182−8189.

(16) Chen, Y.; Tian, G.; Pan, K.; Tian, C.; Zhou, J.; Zhou, W.; Ren, Z.; Fu, H. In Situ Controlled Growth of Well-Dispersed Gold Nanoparticles in TiO_2 Nanotube Arrays as RecyclableSubstrates for Surface-Enhanced Raman Scattering. *Dalton Trans.* **2012**, *41*, 1020−1026.

(17) Li, X.; Chen, G.; Yang, L.; Jin, Z.; Liu, J. Multifunctional Au-Coated TiO_2 Nanotube Arrays as Recyclable SERS Substrates for Multifold Organic Pollutants Detection. *Adv. Funct. Mater.* **2010**, *20*, 2815−2824.

(18) Chen, L.; Luo, L.; Chen, Z.; Zhang, M.; Zapien, J. A.; Lee, C. S.; Lee, S. T. ZnO/Au Composite Nanoarrays As Substrates for Surface-Enhanced Raman Scattering Detection. *J. Phys. Chem. C* **2010**, *114*, 93−100.

(19) Shahar, C.; Levi, R.; Cohen, S. R.; Tenne, R. Gold Nanoparticles as Surface Defect Probes for WS_2 Nanostructures. *J. Phys. Chem. Lett.* **2010**, *1*, 540−543.

(20) Sadan, M. B.; Houben, L.; Enyashin, A. N.; Seifert, G.; Tenne, R. Atom by Atom: HRTEM Insights Into Inorganic Nanotubes and Fullerene-Like Structures. *Proc. Natl. Acad. Sci. U.S.A.* **2008**, *105*, 15643−15648.

(21) Houben, L.; Enyashin, A. N.; Feldman, Y.; Rosentsveig, R.; Stroppa, D. G.; Bar-Sadan, M. Diffraction from Disordered Stacking Sequences in MoS_2 and WS_2 Fullerenes and Nanotubes. *J. Phys. Chem. C* **2012**, *116*, 24350−24357.

(22) Krause, M.; Mucklich, A.; Zak, A.; Seifert, G.; Gemming, S. High Resolution TEM Study of WS_2 Nanotubes. *Phys. Status Solidi B* **2011**, *248*, 2716−2719.

(23) Enyashin, A. N.; Gemming, S.; Bar-Sadan, M.; Popovitz-Biro, R.; Hong, S. Y.; Prior, Y.; Tenne, R.; Seifert, G. Structure and Stability of Molybdenum Sulfide Fullerenes. *Angew. Chem., Int. Ed.* **2007**, *46*, 623−627.

(24) Zak, A.; Sallacan-Ecker, L.; Margolin, A.; Genut, M.; Tenne, R. Insight into the Growth Mechanism of WS_2 Nanotubes in the Scaled-Up Fluidized-Bed Reactor. *NANO* **2009**, *4*, 91−98.

(25) Zak, A.; Sallacan-Ecker, L.; Efrati, R.; Drangai, L.; Fleischer, N.; Tenne, R. Large-Scale Synthesis of WS_2 Multiwall Nanotubes and Their Dispersion, an Update. *Sens. Transducers J.* **2011**, *12* (Special issue, Oct), 1−10.

(26) Feldman, Y.; Wasserman, E.; Srolovitz, D. J.; Tenne, R. High-Rate, Gas-Phase Growth of MoS_2 Nested Inorganic Fullerenes and Nanotubes. *Science* **1995**, *267*, 222−225.

(27) Feldman, Y.; Frey, G. L.; Homyonfer, M.; Lyakhovitskaya, V.; Margulis, L.; Cohen, H.; Hodes, G.; Hutchison, J. L.; Tenne, R. Bulk Synthesis of Inorganic Fullerene-Like MS_2 (M = Mo, W) from the Respective Trioxides and the Reaction Mechanism. *J. Am. Chem. Soc.* **1996**, *118*, 5362−5367.

(28) Zhang, W.; Ge, S.; Wang, Y.; Rafailovich, M. H.; Dhez, O.; Winesett, D. A.; Ade, H.; Shafi, K. V. P. M.; Ulman, A.; Popovitz-Biro, R.; et al. Use of Functionalized WS_2 Nanotubes to Produce New Polystyrene/Polymethylmethacrylate Nanocomposites. *Polymer* **2003**, *44*, 2109−2115.

(29) Shahar, C.; Zbaida, D.; Rapoport, L.; Cohen, H.; Bendikov, T.; Tannous, J.; Dassenoy, F.; Tenne, R. Surface Functionalization of WS_2 Fullerene-Like Nanoparticles. *Langmuir* **2010**, *26*, 4409−4414.

(30) Kreizman, R.; Schwartz, O.; Deutsch, Z.; Itzhakov, S.; Zak, A.; Cohen, S. R.; Tenne, R.; Oron, D. Semiconductor Quantum Dot−Inorganic Nanotube Hybrids. *Phys. Chem. Chem. Phys.* **2012**, *14*, 4271−4275.

(31) Kreizman, R.; Hong, S. Y.; Sloan, J.; Popovitz-Biro, R.; Albu-Yaron, A.; Tobias, G.; Ballesteros, B.; Davis, B. G.; Green, M. L. H.; Tenne, R. Core−Shell PbI_2@WS_2 Inorganic Nanotubes from Capillary Wetting. *Angew. Chem., Int. Ed.* **2009**, *48*, 1230−1233.

(32) Kreizman, R.; Enyashin, A. N.; Deepak, F. L.; Albu-Yaron, A.; Popovitz-Biro, R.; Seifert, G.; Tenne, R. Synthesis of Core−Shell Inorganic Nanotubes. *Adv. Funct. Mater.* **2010**, *20*, 2459−2468.

(33) Tahir, M. N.; Yella, A.; Sahoo, J. K.; Annal-Therese, H.; Zink, N.; Tremel, W. Synthesis and Functionalization of Chalcogenide Nanotubes. *Phys. Status Solidi B* **2010**, *247*, 2338−2363.
(34) Tahir, M. N.; Zink, N.; Eberhardt, M.; Therese, H. A.; Kolb, U.; Theato, P.; Tremel, W. Overcoming the Insolubility of Molybdenum Disulfide Nanoparticles Through a High Degree of Sidewall Functionalization Using Polymeric Chelating Ligands. *Angew. Chem., Int. Ed.* **2006**, *45*, 4809−4815.
(35) Tahir, M. N.; Zink, N.; Eberhardt, M.; Therese, H. A.; Faiss, S.; Janshoff, A.; Kolb, U.; Theato, P.; Tremel, W. Hierarchical Assembly of TiO_2 Nanoparticles on WS_2 Nanotubes Achieved Through Multifunctional Polymeric Ligands. *Small* **2007**, *3*, 829−834.
(36) Tahir, M. N.; Natalio, F.; Therese, H. A.; Yella, A.; Metz, N.; Shah, M. R.; Mugnaioli, E.; Berger, R.; Theato, P.; Schröder, H.-C.; et al. Enzyme-Mediated Deposition of a TiO_2 Coating Onto Biofunctionalized WS_2 Chalcogenide Nanotubes. *Adv. Funct. Mater.* **2009**, *19*, 285−291.
(37) Tahir, M. N.; Yella, A.; Therese, H. A.; Mugnaioli, E.; Panthofer, M.; Khan, H. U.; Knoll, W.; Kolb, U.; Tremel, W. Synthesis of Hierarchically Grown ZnO@NT-WS_2 Nanocomposites. *Chem. Mater.* **2009**, *21*, 5382−5387.
(38) Sahoo, J. K.; Tahir, M. N.; Yella, A.; Schladt, T. D.; Mugnaoli, E.; Kolb, U.; Tremel, W. Reversible Self-Assembly of Metal Chalcogenide/Metal Oxide Nanostructures Based on Pearson Hardness. *Angew. Chem., Int. Ed.* **2010**, *49*, 7578−7582.
(39) Sahoo, J. K.; Tahir, M. N.; Hoshyargar, F.; Nakhjavan, B.; Branscheid, R.; Kolb, U.; Tremel, W. Molecular Camouflage: Making Use of Protecting Groups To Control the Self-Assembly of Inorganic Janus Particles Onto Metal−Chalcogenide Nanotubes by Pearson Hardness. *Angew. Chem., Int. Ed.* **2011**, *50*, 12271−12275.
(40) Cheng, F.; Chen, J.; Gou, X. MoS_2−Ni Nanocomposites as Catalysts for Hydrodesulfurization of Thiophene and Thiophene Derivatives. *Adv. Mater.* **2006**, *18*, 2561−2564.
(41) Tsverin, Y.; Popovitz-Biro, R.; Feldman, Y.; Tenne, R.; Komarneni, M. R.; Yu, Z.; Chakradhar, A.; Sand, A.; Burghaus, U. Synthesis and Characterization of WS_2 Nanotube Supported Cobalt Catalyst for Hydrodesulfurization. *Mater. Res. Bull.* **2012**, *47*, 1653−1660.
(42) Tsverin, Y.; Livneh, T.; Rosentsveig, R.; Zak, A.; Pinkas, I.; Tenne, R. Photocatalysis with Hybrid Co-Coated WS_2 Nanotubes. *Nanomater. Energy* **2012**, *2*, 25−34.
(43) Rosentsveig, R.; Gorodnev, A.; Feuerstein, N.; Friedman, H.; Zak, A.; Fleischer, N.; Tannous, J.; Dassenoy, F.; Tenne, R. Fullerene-Like MoS_2 Nanoparticles and Their Tribological Behavior. *Tribol. Lett.* **2009**, *36*, 175−182.
(44) ICDD Products-PDF-4. http://www.icdd.com/products/pdf4.htm (accessed May 19, 2012).
(45) Bar-Sadan, M.; Enyashin, A. N.; Gemming, S.; Popovitz-Biro, R.; Hong, S. Y.; Prior, Y.; Tenne, R.; Seifert, G. Structure and Stability of Molybdenum Sulfide Fullerenes. *J. Phys. Chem. B* **2006**, *110*, 25399−25410.
(46) Jaegermann, W.; Ohuchi, F. S.; Parkinson, B. A. Interaction of Cu, Ag and Au with van der Waals Faces of WS_2 and SnS_2. *Surf. Sci.* **1988**, *201*, 211−227.
(47) McMenamin, J. C.; Spicer, W. E. Photoemission Studies of Layered Transition-Metal Dichalcogenides: MoS_2. *Phys. Rev. B* **1977**, *16*, 5474−5487.
(48) Liu, K.-K.; Zhang, W.; Lee, Y.-H.; Lin, Y.-C.; Chang, M.-T; Su, C.-Y.; Chang, C.-S.; Li, H.; Shi, Y.; Zhang, H.; et al. Growth of Large-Area and Highly Crystalline MoS_2 Thin Layers on Insulating Substrates. *Nano Lett.* **2012**, *12*, 1538−1544.
(49) Reiss, H.; Heller, A. The Absolute Potential of the Standard Hydrogen Electrode: A New Estimate. *J. Phys. Chem.* **1985**, *89*, 4207−4213.
(50) Choi, H. C.; Shim, M.; Bangsaruntip, S.; Dai, H. Spontaneous Reduction of Metal Ions on the Sidewalls of Carbon Nanotubes. *J. Am. Chem. Soc.* **2002**, *124*, 9058−9059.
(51) Kong, B. S.; Geng, J. X.; Jung, H. T. Layer-by-Layer Assembly of Graphene and Gold Nanoparticles by Vacuum Filtration and Spontaneous Reduction of Gold Ions. *Chem. Commun.* **2009**, 2174−2176.
(52) Shin, H.-J.; Choi, W. M.; Choi, D.; Han, G. H.; Yoon, S.-M.; Park, H.-K.; Kim, S.-W.; Jin, Y. W.; Lee, S. Y.; Kim, J. M.; et al. Control of Electronic Structure of Graphene by Various Dopants and Their Effects on a Nanogenerator. *J. Am. Chem. Soc.* **2010**, *132*, 15603−15609.
(53) Kim, J.; Byun, S.; Smith, A. J.; Yu, J.; Huang, J. Enhanced Electrocatalytic Properties of Transition Metal Dichalcogenides Sheets by Spontaneous Gold Nanoparticle Decoration. *J. Phys. Chem. Lett.* **2013**, *4*, 1227−1232.
(54) Golub, A. S.; Zubavichus, Y. V.; Lenenko, N. D.; Slovokhotov, Yu.L.; Danot, M.; Novikov, Yu.N. Ternary Metal Sulfides M_zMoS_2: Synthesis Using Single-Layer Dispersions of Molybdenum Disulfide and Study of the Structure. *Russ. Chem. Bull., Int. Ed.* **2001**, *50*, 2293−2303.
(55) Frey, G. L.; Elani, S.; Homyonfer, M.; Feldman, Y.; Tenne, R. Optical-Absorption Spectra of Inorganic Fullerenelike MS_2 (M = Mo, W). *Phys. Rev. B* **1988**, *57*, 6666−6671.
(56) Yadgarov, L.; Choi, C. L.; Sedova, A.; Cohen, A.; Rosentsveig, R.; Bar-Elli, O.; Oron, D.; Dai, H.; Tenne, R. Dependence of the Absorption and Optical Surface Plasmon Scattering of MoS_2 Nanoparticles on Aspect Ratio, Size and Media. *ACS Nano* 2014, submitted.
(57) Link, S.; El-Sayed, M. A. Size and Temperature Dependence of the Plasmon Absorption of Colloidal Gold Nanoparticles. *J. Phys. Chem. B* **1999**, *103*, 4212−4217.
(58) Fleger, Y.; Rosenbluh, M.; Strelniker, Y. M.; Bergman, D. J.; Lagarkov, A. N. Controlling the Optical Spectra of Gold Nano-Islands by Changing the Aspect Ratio and the Inter-Island Distance: Theory and Experiment. *Eur. Phys. J. B* **2011**, *81*, 85−93.
(59) Ting, L.; Li, Y.; Zhi-Xin, L.; Gang, S.; Kai, Z. Controlling Optical Properties of Periodic Gold Nanoparticle Arrays by Changing the Substrate, Topologic Shapes of Nanoparticles, and Polarization Direction of Incident Light. *Chin. Phys. B* **2011**, *20*, 087805.
(60) Jiang, C.; Markutsya, S.; Tsukruk, V. V. Collective and Individual Plasmon Resonances in Nanoparticle Films Obtained by Spin-Assisted Layer-by-Layer Assembly. *Langmuir* **2004**, *20*, 882−890.
(61) Furube, A.; Du, L.; Hara, K.; Katoh, R.; Tachiya, M. Ultrafast Plasmon-Induced Electron Transfer from Gold Nanodots Into TiO_2 Nanoparticle. *J. Am. Chem. Soc.* **2007**, *129*, 14852−14853.
(62) Khon, E.; Mereshchenko, A.; Tarnovsky, A. N.; Acharya, K.; Klinkova, A.; Hewa-Kasakarage, N. N.; Nemitz, I.; Zamkov, M. Suppression of the Plasmon Resonance in Au/CdS Colloidal Nanocomposites. *Nano Lett.* **2011**, *11*, 1792−1799.